Cancer Immunology, Immunotherapy (2023) 72:2151–2168
https://doi.org/10.1007/s00262-023-03407-5

RESEARCH

Mitochondrial C1QBP is essential for T cell antitumor function by maintaining mitochondrial plasticity and metabolic fitness

Hui Tian[1,2,3] · Dafei Chai[1,2,3] · Gang Wang[1,2,3] · Qiping Wang[5] · Nan Sun[1,2,3] · Guan Jiang[6] · Huizhong Li[1,2,3] · Jingyuan Song[7] · Lin Fang[1,2,3] · Meng Wang[1,2,3] · Zengli Guo[1,4] · Junnian Zheng[2,3]

Received: 25 February 2022 / Accepted: 11 February 2023 / Published online: 25 February 2023

Abstract

The metabolic stress present in the tumor microenvironment of many cancers can attenuate T cell antitumor activity, which is intrinsically controlled by the mitochondrial plasticity, dynamics, metabolism, and biogenesis within these T cells. Previous studies have reported that the complement C1q binding protein (C1QBP), a mitochondrial protein, is responsible for maintenance of mitochondrial fitness in tumor cells; however, its role in T cell mitochondrial function, particularly in the context of an antitumor response, remains unclear. Here, we show that C1QBP is indispensable for T cell antitumor immunity by maintaining mitochondrial integrity and homeostasis. This effect holds even when only one allele of *C1qbp* is functional. Further analysis of C1QBP in the context of chimeric antigen receptor (CAR) T cell therapy against the murine B16 melanoma model confirmed the cell-intrinsic role of C1QBP in regulating the antitumor functions of CAR T cells. Mechanistically, we found that *C1qbp* knocking down impacted mitochondrial biogenesis via the AMP-activated protein kinase (AMPK)/peroxisome proliferator-activated receptor gamma coactivator 1-alpha signaling pathway, as well as mitochondrial morphology via the phosphorylation of mitochondrial dynamics protein dynamin-related protein 1. In summary, our study provides a novel mitochondrial target to potentiate the plasticity and metabolic fitness of mitochondria within T cells, thus improving the immunotherapeutic potential of these T cells against tumors.

Keywords Antitumor immunity · C1QBP · Mitochondrial biogenesis · Mitochondrial dynamics · Mitochondrial metabolism · Mitochondrial plasticity

Introduction

Mitochondria are highly plastic organelles which are critical in modulating T cell development, fate determination, and antitumor responses [1–4]. In order to functional desirably, it is critical for the mitochondria within T cell to remain plastic and metabolically fit in response to a variety of metabolic perturbations. Mitochondrial plasticity including mitochondrial dynamics, metabolism and biogenesis is tightly linked to mitochondrial structure, function, activity,

✉ Zengli Guo
zlguo@email.unc.edu

✉ Junnian Zheng
jnzheng@xzhmu.edu.cn

1 Cancer Institute, Xuzhou Medical University, Xuzhou 221002, Jiangsu, People's Republic of China

2 Center of Clinical Oncology, Affiliated Hospital of Xuzhou Medical University, Xuzhou 221002, Jiangsu, People's Republic of China

3 Jiangsu Center for the Collaboration and Innovation of Cancer Biotherapy, Cancer Institute, Xuzhou Medical University, Xuzhou 221002, Jiangsu, People's Republic of China

4 Lineberger Comprehensive Cancer Center, School of Medicine, University of North Carolina, Chapel Hill, NC, USA

5 Jiangyin Clinical Medical College, Jiangsu University, Jiangyin City 214400, Jiangsu, People's Republic of China

6 Department of Dermatology, Affiliated Hospital of Xuzhou Medical University, Xuzhou 221002, Jiangsu, People's Republic of China

7 School of Nursing, Xuzhou Medical University, Xuzhou 221002, People's Republic of China

and homeostasis [2, 4–7]. Robust mitochondrial plasticity endows T cells, and especially tumor-infiltrating T lymphocytes (TILs), with persistent and durable antitumor function, while impaired mitochondrial plasticity causes TILs to exhibit metabolic insufficiency, exhaustion, and hypofunction [6, 8, 9]. However, the causal relationship between T cell mitochondrial plasticity and T cell antitumor immune function in response to metabolic stress of the tumor microenvironment (TME) still remains poorly understood.

The complement C1q binding protein (C1QBP), predominantly located in the mitochondrial matrix, has been correlated with cellular bioenergetics and mitochondrial function in tumor cells. Specifically, C1QBP has been implicated in metabolic reprogramming via regulation of mitochondrial morphology and metabolism, which is further connected to tumor transformation and metastasis [10–14]. Nevertheless, metabolic adaptation via the mitochondria is required not only for tumor malignant progression but also for tumor-specific T cells to perform their antitumor immune responses [15–17]. Given that C1QBP is indispensable for mitochondrial structure and function, exploring the exact role of C1QBP in regulation of T cell mitochondrial plasticity and the subsequent impact of antitumor immunity will be of interest.

Mitochondria are constantly performing cycles of fission and fusion in order to meet the ever-changing metabolic needs of their host cells [18–22]. Among the many other impacts of this behavior, increasing evidence has suggested that such mitochondrial dynamics help to determine T cells' fate through metabolic programming. At the same time, it has been shown that mitochondrial fusion in T cells can improve adoptive antitumor cell therapy responses [2, 3]. In this study, we wanted to interrogate the effect and mechanism of C1QBP on the mitochondrial dynamics of T cells. Besides, the previous study reported that C1QBP has also been implicated in regulation of mitochondrial oxidative phosphorylation (OXPHOS): *C1qbp*-deficient mouse embryonic fibroblasts (MEFs) showed impaired OXPHOS and ATP production, which resulted in the delayed embryonic development [23]. However, whether C1QBP could be involved in the manipulation of T cell metabolic fitness through mitochondria-mediated OXPHOS still remains unclear.

Mitochondrial biogenesis has not only been implicated in the maintenance of mitochondrial mass, but also in the regulation of T cell antitumor immune function. TILs notoriously exhibit persistent loss of mitochondrial biogenesis in both human patients and mouse models, while proper maintenance of mitochondrial biogenesis is required to recover T cell antitumor responses [24, 25]. Although C1QBP is reported to be associated with the formation of mitochondrial ribosomes and mitochondrial DNA (mtDNA)-encoded mitochondrial protein translation [23, 26], here we want to explore whether C1QBP regulates T cell mitochondrial biogenesis and mass to impact TILs exhaustion in the nutrient-and oxygen-deprived TME.

Finally, in order to assess the potential role of C1QBP in CAR T cell therapy, we evaluated the impact of C1QBP on mitochondrial plasticity and further delineated the role of C1QBP on CAR T cells tumor infiltration, central memory cell formation, and exhausted phenotype development, thus impacting their antitumor immune response.

Materials and methods

Mice

C1qbp heterozygous mice were donated by Dr. Yanping Zhang from the Department of Radiation Oncology at Lineberger Comprehensive Cancer Center, University of North Carolina, USA. *C1qbp* heterozygous mice were generated as previously described [27]. All mice were housed and bred in the specific pathogen-free (SPF) animal facility of the Experimental Animal Center in Xuzhou Medical University. All experimental animal procedures were performed in compliance with institutional ethical requirements and approved by the Committee of Xuzhou Medical University for the Use and Care of Animals.

Immunoblot analysis

Lysates of T cells were prepared in lysis buffer (50 mM Tris–HCl, pH 7.4, 150 mM NaCl, 2 mM EDTA, 0.2% Triton X-100, 0.5% NP-40, and protease inhibitor cocktail). Samples were resolved by SDS/PAGE (12% gel) and transferred to nitrocellulose membranes. The transferred membranes were blocked with 5% (w/v) non-fat dried skimmed milk powder in PBST and immunoblotted using the commercially available primary antibodies listed below. Membranes were then washed with PBST, incubated with the appropriate HRP (horseradish peroxidase)-conjugated secondary antibodies in 5% (w/v) non-fat dried skimmed milk powder/PBST, and visualized using enhanced chemiluminescence reagents (Proteintech) according to the manufacturer's instructions.

Immunofluorescence

For immunofluorescence imaging, T cells were fixed in 4% paraformaldehyde for 15 min at room temperature and permeabilized in 0.2% Triton X-100 for 5 min at 4 °C. Fixed and permeabilized cells were blocked for 30 min in 0.5% BSA blocking buffer diluted in PBS, incubated with the appropriate primary antibody overnight at 4 °C, and then incubated with Alexa Fluor secondary antibodies (Life

Technology Inc.) for 1 h at room temperature. Nuclei were stained by (4′,6-diamidino-2-phenylindole) (DAPI). All stained cells were mounted with fluorescence mounting medium (Dako, Carpinteria, CA, USA) and then were observed using the ZEISS LSM 880 confocal fluorescence microscope. Images were analyzed with ImageJ software.

Flow cytometry and analyzation

For preparation of tumor single cell suspensions, tumor tissues from *C1qbp*$^{+/+}$ and *C1qbp*$^{\pm}$ mice were mechanically dissected and washed with PBS. The tumor cell suspension was passed through a sterile 40 μm Nylon Filter (BD Falcon). The single cell suspension was then stained by PerCP-anti-mouse-CD4 and APC-anti-mouse-CD8α antibodies to detect the percentage of tumor-infiltrating $CD4^+$ and $CD8^+$ T cells. Next, in order to examine tumor-infiltrating T cell exhaustion, the single-cell suspension was also stained by PE-anti-mouse-PD-1, PE-anti-mouse-LAG-3, PE-anti-mouse-Tim-3 antibodies, respectively. In parallel, *C1qbp*$^{+/+}$ and *C1qbp*$^{\pm}$ T cells were activated to anti-CD3/CD28 antibodies or tumor single-cell suspensions, and were stained with MitoTracker Green (M7514, ThermoFisher) or MitoTracker Deep Red (M22426, ThermoFisher) to measure mitochondrial mass. Stained cells were detected by the FACS CantoTM II Flow Cytometer (BD biosciences), and FACS data were analyzed using FlowJo software (TreeStar).

Seahorse extracellular flux analysis

For analysis of the metabolic phenotype of *C1qbp*$^{+/+}$ and *C1qbp*$^{\pm}$ T cells, oxygen consumption rate (OCR) and extracellular acidification rate (ECAR) were measured using the Seahorse XF-96 metabolic extracellular flux analyzer (Seahorse Bioscience). FACS-sorted T cells were planted in a 24-well plate coated with anti-CD3ε/CD28 antibodies and cultured with RPMI-1640 medium for 48 h. Activated T cells were then collected and spun on poly-D-lysine coated seahorse 96 well plates (2×10^5 cells per well) and preincubated at 37 °C for a minimum of 45 min in the absence of CO_2. Cellular OCR (pmol/min) was measured under basal conditions and following treatment with 1 μM oligomycin, 2 μM trifluoromethoxy carbonyl cyanide phenylhydrazone (FCCP), 0.5 μM rotenone, and 0.5 μM antimycin (all from Sigma-Aldrich). Real-time analysis of extracellular oxygen and pH was conducted in a standard humidified incubator with 5% CO_2. Mitochondrial function parameters of basal respiratory capacity, maximal respiratory capacity, proton leak, oxidative ATP turnover, and spare respiratory capacity were determined. At the same time, ECAR (mpH/min) was recorded under basal conditions and following the addition of 10 mM glucose, 1 μM oligomycin, and 50 mM 2-deoxyglucose (2-DG). Glycolysis, glycolytic capacity, and glycolytic reserve were determined. The related quantification was analyzed in duplicate for at least three independent experiments.

qRT-PCR analysis of mRNA

Total RNA was isolated from T cells by TRIzol reagent (Invitrogen) following manufacturer's instruction, and then reverse-transcribed into cDNA with HiScript II Q RT SuperMix (Vazyme Biotech Co.). Quantitative real-time PCR was performed on LightCycler 96 real-time PCR system (Roche life Science) with AceQ qPCR SYBR Green Master Mix kit (Vazyme Biotech Co.). The relative mRNA expression of indicated genes was calculated based on the expression of β-actin. Ct values for each analyzed gene were normalized to β-actin and adjusted for amplification efficiency.

Primers to detect β-actin: (FW) 5′-GGGCATCCTGACCCTCAAG-3′,

(RV) 5′- TCCATGTCGTCCCAGTTGGT-3′,

PGC-1α: (FW) 5′-GGATATACTTTACGCAGGTCGA-3′,

(RV) 5′-CGTCTGAGTTGGTATCTAGGTC-3′,

Complex I(ND-1): (FW) 5′-CTAATCGCCATAGCCTTCCTAA-3′,

(RV) 5′-GTTGTTAAAGGGCGTATTGGTT-3′,

Complex II(SDHC): (FW) 5′-TTCTGGAAGAAGAACACGAGTT-3′,

(RV) 5′-GGGAAGACAAGCACAAACTTAG-3′,

Complex III(UQCRC1): (FW) 5′-CGCACAGACTTGACTGACTACCTC-3′,

(RV) 5′-AGGCACGGCATCTTCTTCATACAC-3′,

Complex IV(COXIV): (FW) 5′-ATGTTCTTCATTGGCTTCACTG-3′,

(RV) 5′-AGTCACGATCGAAAGTATGAGG-3′.

Construction of targeted huB7-H3 CAR T cells

In order to prepare targeted huB7-H3 CAR T cells, we first constructed the retroviruses containing huB7-H3 CAR. Procedures and conditions for construction of the targeted huB7-H3 CAR retroviruses were previously described [28]. Next, murine T cells were isolated by Pan T magnetic Microbeads (Miltenyi Biotec) from splenocytes obtained from *C1qbp*$^{+/+}$ and *C1qbp*$^{\pm}$ mice and then stimulated on plates coated with anti-CD3ε/CD28 antibodies for 24 h. Activated murine T cells were transduced with the above retroviral supernatants using retronectin-coated plates (Takara Bio Inc., Shiga, Japan). The transfection of murine T cells was performed according to previous protocols [29]. After removal from the retronectin-coated plates, T cells were expanded in complete RPMI-1640 medium supplemented with 10% FBS, 4 mM L-glutamine, 1% penicillin/streptomycin, 75 μM β-mercaptoethanol, 2 ng/

mL IL-2, 10 ng/mL IL-7, and 5 ng/mL IL-15. After 48 h, CAR T cells targeting huB7-H3 were collected for use in the following in vivo and in vitro experiments.

Murine melanoma B16 cells expressing huB7-H3 antigen

To establish murine melanoma B16 cells stably expressing huB7-H3 antigen (huB7-H3-B16 cells), B16 cells were transduced with the lentiviral particles carrying the open reading frame (ORF) of 4Ig-B7-H3 (GenBank: NM_001024736), firefly luciferase (Luc), and the green fluorescent protein (GFP). 48 h later, the positive huB7-H3-B16 cells expressing high levels of huB7-H3 and GFP were detected and sorted using the FACSAria III Cell Sorter (BD biosciences).

ELISA

CAR T cells targeting huB7-H3 were co-cultured with huB7-H3 B16 tumor cells (2×10^5 cells/well) in 24-well plates at different effector to target ratios ($E{:}T=1{:}2$ or 1:1) without the addition of exogenous cytokines. After 18 h, the supernatant was collected and cytokines IFN-γ and TNF-α were measured in duplicate by specific ELISA kits (Proteintech) following manufacturer's instructions.

Melanoma B16 subcutaneous xenograft mouse model

Murine melanoma B16 cells (2×10^5) expressing firefly luciferase (Luc) were injected subcutaneously into the flanks of 2-month-old female *C1qbp*$^{\pm}$ and *C1qbp*$^{+/+}$ mice on Day 0. To monitor tumor growth, tumor volumes (width × length × width/2; cm^3) from *C1qbp*$^{\pm}$ and *C1qbp*$^{+/+}$ mice were measured with a vernier caliper throughout tumor progression. On Day 24, bioluminescent images of *C1qbp*$^{\pm}$ and *C1qbp*$^{+/+}$ mice bearing B16 tumors were recorded through the Night OWL II LB 983 In Vivo Imaging System (Berthold Technology, German). On Day 25, mice were humanely euthanized by CO_2 asphyxiation, and tumor tissues were collected for downstream experiments or fixed in formalin for immunohistochemistry.

Melanoma huB7-H3-B16 subcutaneous xenograft mouse model

Murine melanoma huB7-H3-B16 cells (2×10^5) expressing human B7-H3 antigen and firefly luciferase (Luc) were injected subcutaneously into one flank of 2-month-old female C57BL/6 mice on Day 0. On Day 15, cyclophosphamide (200 mg/kg) was injected intraperitoneally for the depletion of endogenous lymphocytes. One day later, 2×10^6 non-transduced T cells (NT), anti-huB7-H3 *C1qbp*$^{+/+}$ CAR T cells, or anti-huB7-H3 *C1qbp* $^{\pm}$ CAR T cells were transferred intravenously into the huB7-H3-B16 tumor-bearing mice. Tumor volumes (width × length × width/2; cm^3) of mice from NT, *C1qbp*$^{\pm}$ and *C1qbp*$^{+/+}$ CAR T groups were measured with a vernier caliper throughout tumor progression. On Days 15 and 22, bioluminescent images were recorded via the Night OWL II LB 983 In Vivo Imaging System, allowing comparison before and after the adoptive transfer of NT or CAR-T cells. Tumor volumes were again measured with the vernier caliper. On Day 25, mice were humanely euthanized by CO_2 asphyxiation, and tumor tissues were collected for downstream experiments or fixed in formalin for immunohistochemistry.

Melanoma huB7-H3-B16 metastasis mouse model

Murine melanoma huB7-H3-B16 cells (3×10^5) expressing huB7-H3 antigen and firefly luciferase (Luc) were injected intravenously into C57BL/6 mice on Day 0. On Day 11, cyclophosphamide (200 mg/kg) was injected intraperitoneally. One day later, 2×10^6 NT, anti-huB7-H3 *C1qbp*$^{+/+}$ CAR T cells, or anti-huB7-H3 *C1qbp* $^{\pm}$ CAR T cells were transferred intravenously into the huB7-H3-B16 tumor-bearing mice. On Days 14 and 20, bioluminescent images were recorded via the Night OWL II LB 983 In Vivo Imaging System. On Day 20, mice were humanely euthanized by CO_2 asphyxiation, and tumor tissues were collected for downstream experiments or fixed in formalin for immunohistochemistry.

Statistical analysis

Data were analyzed using Graph Pad Prism 6.0 software (La Jolla, CA). Statistical comparisons were performed using the Student's *t*-test. A P-value <0.05 was considered statistically significant. All results are presented as the mean ± standard deviation.

Results

Compromised antitumor immune response in *C1qbp* heterozygous mice

Given that C1QBP homozygous deletion results in early embryonic lethality [23], we wanted to investigate whether disruption of just one allele of *C1qbp* would impact T cell development and homeostasis. First, we observed that C1QBP protein levels of *C1qbp*$^{\pm}$ mouse were significantly decreased relative to wild-type in a variety of organs including brain, lung, liver, colon, and kidney (S. Fig. 1A). Moreover, we isolated the T cells of *C1qbp*$^{\pm}$

and *C1qbp*$^{+/+}$ mice, and found that *C1qbp*$^{\pm}$ T cells also exhibited significantly decreased levels of C1QBP protein in response to stimulation with anti-CD3/CD28 antibodies (S. Fig. 1B). At the same time, we found that the relative percentages of CD4^{+} and CD8^{+} T cells in the spleen, lymph nodes, and blood were comparable in both *C1qbp*$^{\pm}$ mice and their *C1qbp*$^{+/+}$ littermates. Additionally, *C1qbp*$^{\pm}$ and *C1qbp*$^{+/+}$ mice had similar immune compartments, including CD44^{hi}CD62L^{lo} effector memory cells and CD44^{lo}CD62L^{hi} naïve T cells (S. Fig. 2). These above data suggest that disruption of one allele of *C1qbp* is unable to significantly alter T cell development and homeostasis in a healthy, non-cancerous context.

However, to further evaluate whether C1QBP might regulate anti-tumor immunity, we injected murine melanoma B16 cells subcutaneously into the flanks of *C1qbp*$^{+/+}$ and *C1qbp*$^{\pm}$ mice, and observed their tumor progression. As shown in Fig. 1A–C, *C1qbp*$^{\pm}$ mice exhibited significantly more severe tumor progression than their *C1qbp*$^{+/+}$ littermates. Uncontrolled tumor progression in *C1qbp*$^{\pm}$ mice was further supported by expression of important tumor cell markers, including increased levels of Ki67 (tumor proliferation) and decreased levels of Puma (apoptosis) (Fig. 1D). Together, these data suggest that a single- allele deletion of *C1qbp* is sufficient to compromise the antitumor immune response.

Knocking down *C1qbp* dampens T cell antitumor responses

To explore the precise role of C1QBP in T cell antitumor immunity, we further investigated the relative proportions of CD44^{hi}CD62L^{hi} central memory and CD44^{hi}CD62L^{lo} effector memory T cells in the tumor and spleen. As shown in

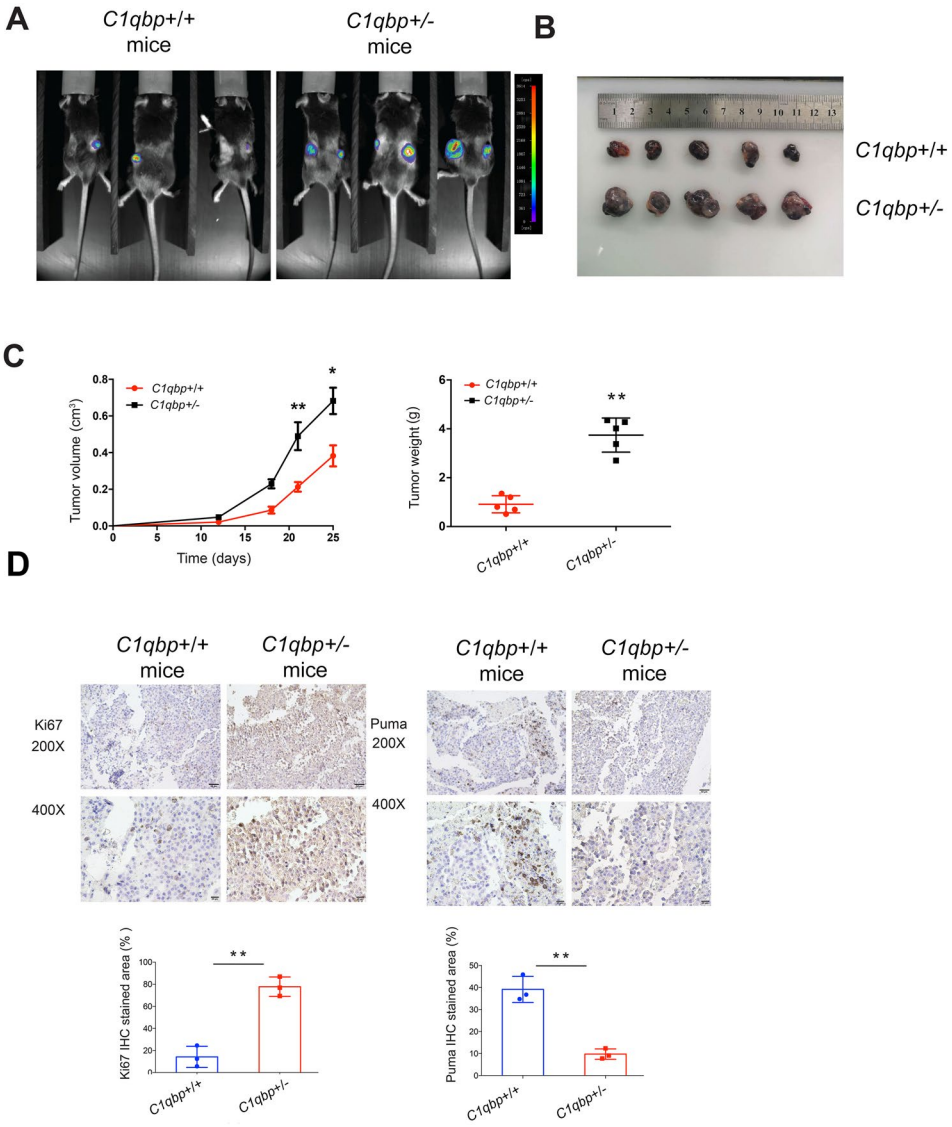

Fig. 1 *C1qbp* knockdown affects tumor progression. Melanoma B16 cells (2×10^5) expressing firefly luciferase (Luc) were injected subcutaneously into the flanks of *C1qbp*$^{+/+}$ and *C1qbp*$^{\pm}$ mice on Day 0 (5 mice/group). **A** In vivo bioluminescent images of *C1qbp*$^{+/+}$ and *C1qbp*$^{\pm}$ mice with B16 tumors on Day 24. **B** In vitro images of B16 tumors collected from the above mice on Day 25. **C** Volumes and weights of B16 tumors. **(D)** Ki67 (proliferation marker) and Puma (pro-apoptotic marker) in B16 tumors were assessed by immunohistochemistry. Scale bars, 50 µm (200×), 20 µm (400×). Bar graphs show the mean ± S.D. of three independent experiments ($n=3$); $^{*}P<0.05$, $^{**}P<0.01$

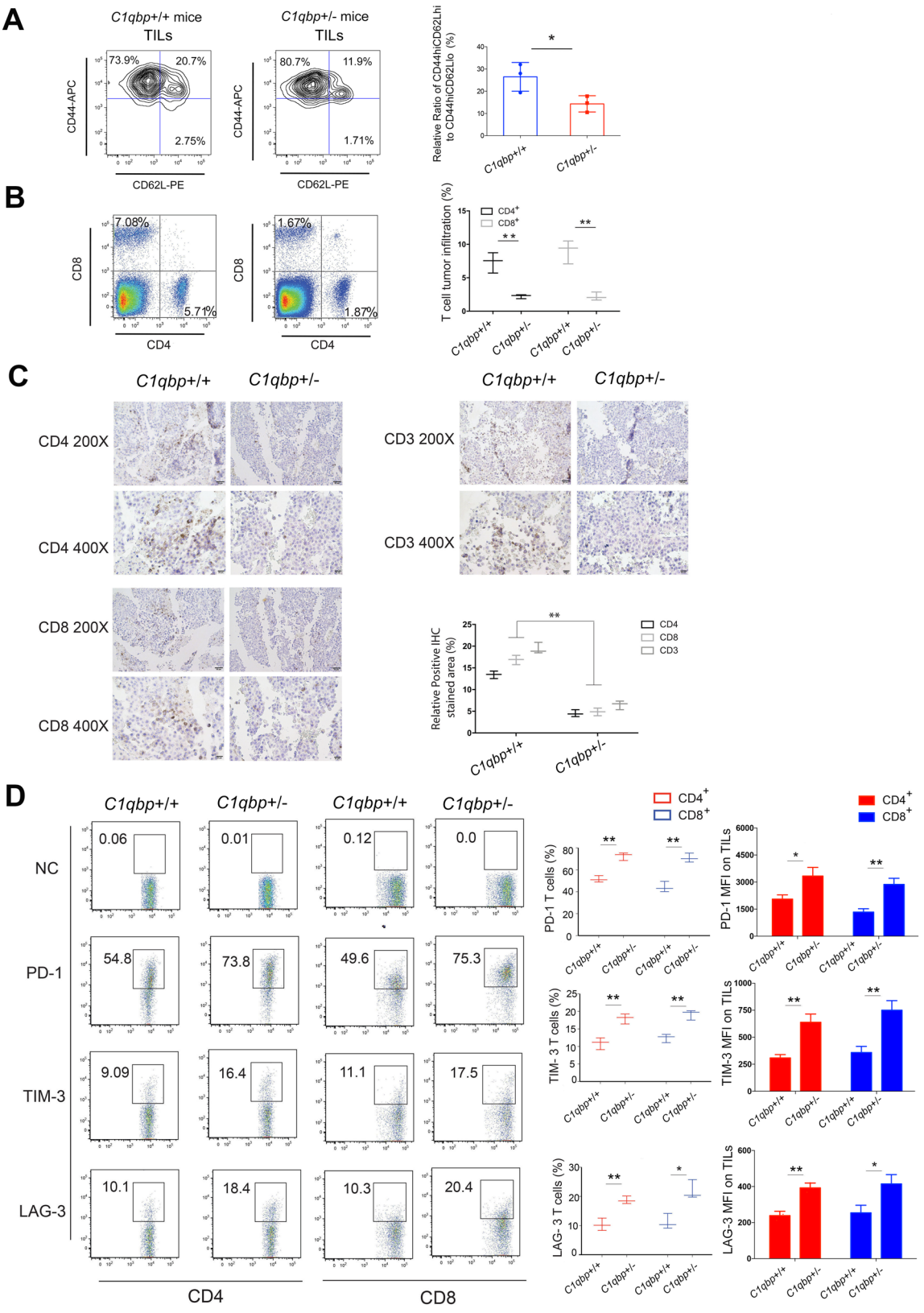
A
C1qbp+/+ mice
TILs
C1qbp+/- mice
TILs
CD44-APC
CD62L-PE
73.9%
20.7%
2.75%
80.7%
11.9%
1.71%
Relative Ratio of CD44hiCD62Lhi to CD44hiCD62Llo (%)
B
CD8
CD4
7.08%
5.71%
1.67%
1.87%
T cell tumor infiltration (%)
CD4+
CD8+
C
C1qbp+/+
C1qbp+/-
CD4 200X
CD4 400X
CD8 200X
CD8 400X
CD3 200X
CD3 400X
Relative Positive IHC stained area (%)
CD4
CD8
CD3
D
NC
PD-1
TIM-3
LAG-3
0.06
0.01
0.12
0.0
54.8
73.8
49.6
75.3
9.09
16.4
11.1
17.5
10.1
18.4
10.3
20.4
PD-1 T cells (%)
TIM- 3 T cells (%)
LAG- 3 T cells (%)
PD-1 MFI on TILs
TIM-3 MFI on TILs
LAG-3 MFI on TILs

◂**Fig. 2** *C1qbp* knockdown impacts T cell antitumor response. **A** Proportions of $CD44^{hi}CD62L^{hi}$ central memory and $CD44^{hi}CD62L^{lo}$ effector memory TILs in B16 tumors from $C1qbp^{+/+}$ and $C1qbp^{\pm}$ mice, as detected by flow cytometry. **B** Relative percentages of $CD4^+$ and $CD8^+$ TILs in B16 tumors from $C1qbp^{+/+}$ and $C1qbp^{\pm}$ mice, as assessed by flow cytometry. **C** Proportions of $CD4^+$, $CD8^+$, and $CD3^+$ TILs in B16 tumors from $C1qbp^{+/+}$ and $C1qbp^{\pm}$ mice, as detected by immunohistochemistry. Scale bars, 50 μm (200×), 20 μm (400×). **D** Exhaustion markers (PD-1, Tim-3, LAG-3) expressed by $CD4^+$ and $CD8^+$ TILs in B16 tumors from $C1qbp^{+/+}$ and $C1qbp^{\pm}$ mice, as analyzed by flow cytometry. Bar graphs show the mean ± S.D. of three independent experiments ($n=3$); $^*P<0.05$, $^{**}P<0.01$

Fig. 2A, Knocking down *C1qbp* led to a moderately lower ratio of $CD44^{hi}CD62L^{hi}$ central memory to $CD44^{hi}CD62L^{lo}$ effector memory T cells in the tumor, while C1QBP deficiency did not alter their proportion in spleen (S. Fig. 3). We further noticed a drastic decrease of T cells in the tumor tissues of $C1qbp^{\pm}$ mice, which was correlated with the low expression of C1QBP in these T cells. As shown in Fig. 2B, the percentage of tumor infiltrating $CD4^+$ T cells in $C1qbp^{\pm}$ mice (1.87%) is dramatically less than that in $C1qbp^{+/+}$ mice (5.71%). Similarly, the percentage of tumor infiltrating $CD8^+$ T cells in $C1qbp^{\pm}$ mice (1.67%) is much lower than that in $C1qbp^{+/+}$ mice (7.08%). Moreover, immunohistochemistry staining also confirmed that knocking down *C1qbp* repressed tumor infiltration by both $CD4^+$ and $CD8^+$ T cells (Fig. 2C).

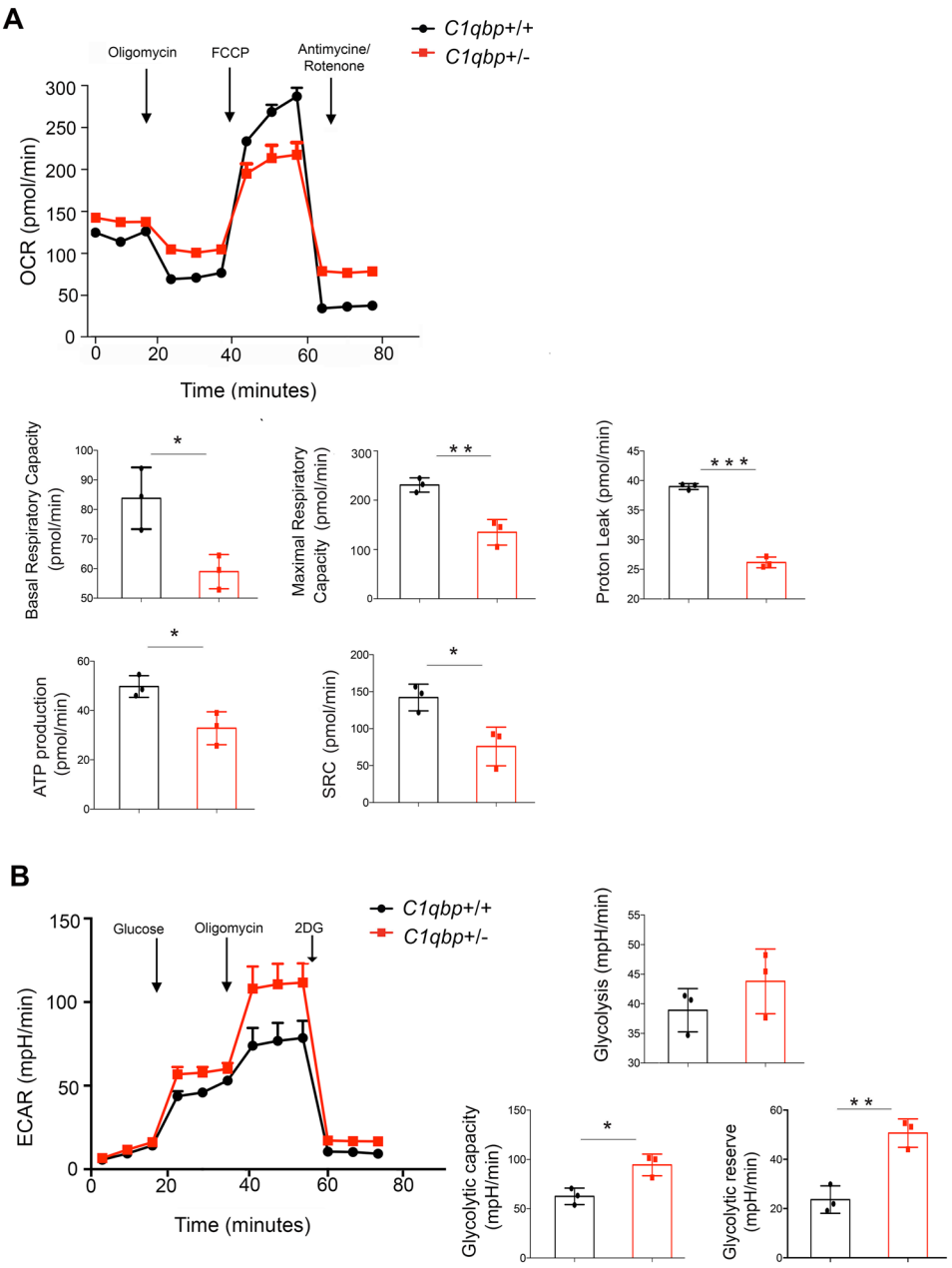

Fig. 3 *C1qbp* knockdown impairs T cell mitochondrial OXPHOS. $C1qbp^{+/+}$ and $C1qbp^{\pm}$ T cells were stimulated with anti-CD3/CD28 antibodies for 48 h. **A** The cellular OCR (pmol/min) was measured under basal conditions and following treatment with 1 μM oligomycin, 2 μM trifluoromethoxy carbonyl cyanide phenylhydrazone (FCCP), 0.5 μM rotenone and 0.5 μM antimycin using the Seahorse Extracellular Flux Analyzer. Basal respiratory capacity, maximal respiratory capacity, proton leak, ATP turnover, and SRC were assessed as different parameters of mitochondrial OXPHOS in $C1qbp^{+/+}$ and $C1qbp^{\pm}$ T cells. Top panel, representative curve; bottom panel, quantification of three independent experiments. **B** The cellular ECAR (mpH/min) of $C1qbp^{+/+}$ and $C1qbp^{\pm}$ T cells was measured under basal conditions and following treatment with 10 mM glucose, 1 μM oligomycin, and 50 mM 2-DG using the Seahorse Extracellular Flux Analyzer. Left panel, representative curve; Right panel, quantification of three independent experiments. The bar graphs show the mean ± S.D. of three independent experiments ($n=3$); $^*P<0.05$, $^{**}P<0.01$, $^{***}P<0.001$

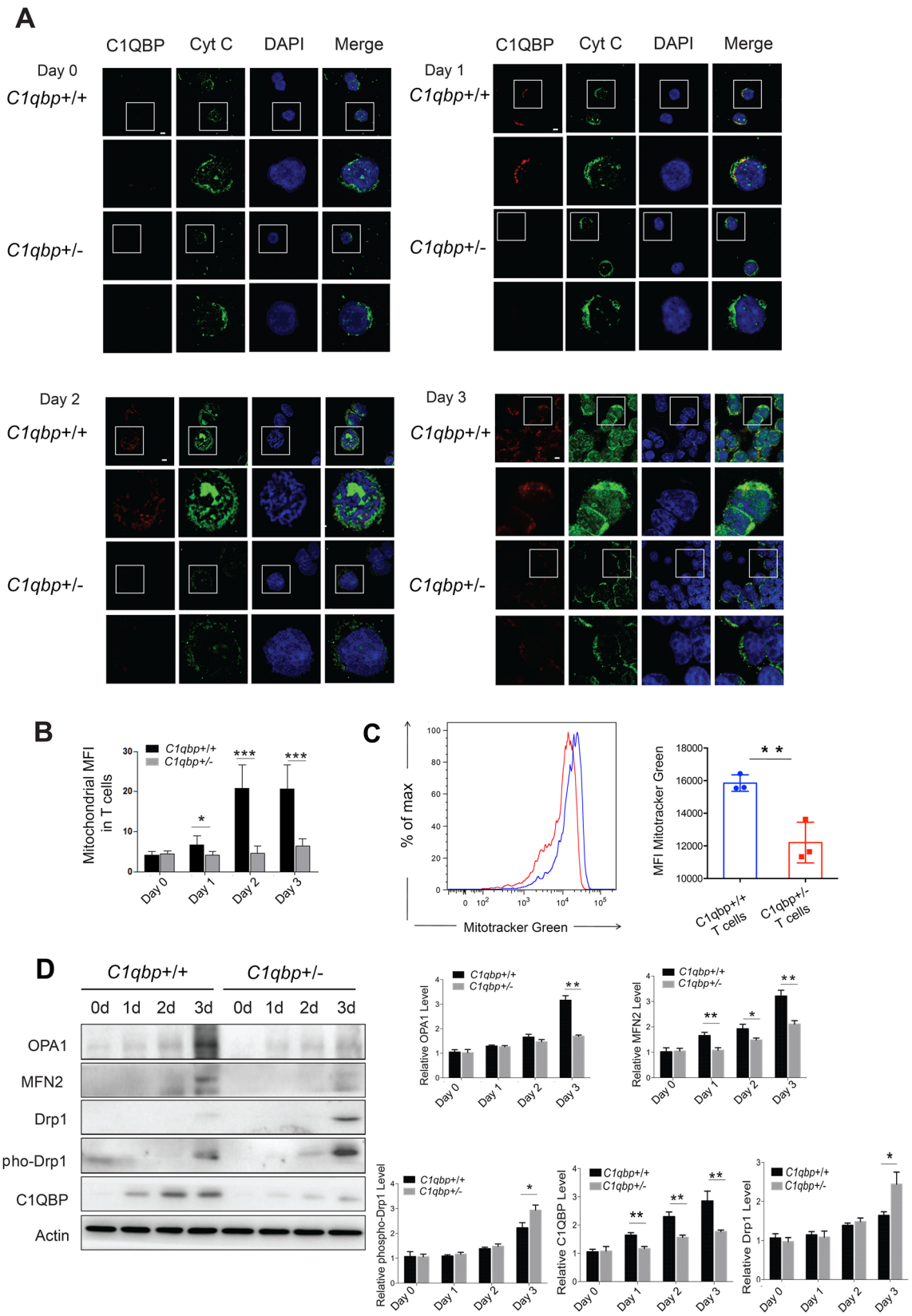
A
C1QBP
Cyt C
DAPI
Merge
Day 0
Day 1
Day 2
Day 3
C1qbp+/+
C1qbp+/-
B
Mitochondrial MFI in T cells
C1qbp+/+
C1qbp+/-
Day 0
Day 1
Day 2
Day 3
C
% of max
Mitotracker Green
MFI Mitotracker Green
C1qbp+/+ T cells
C1qbp+/- T cells
D
C1qbp+/+
C1qbp+/-
0d 1d 2d 3d
OPA1
MFN2
Drp1
pho-Drp1
C1QBP
Actin
Relative OPA1 Level
Relative MFN2 Level
Relative phospho-Drp1 Level
Relative C1QBP Level
Relative Drp1 Level

◂**Fig. 4** *C1qbp* knockdown alters T cell mitochondrial morphologies. **A** T cells isolated from $C1qbp^{+/+}$ and $C1qbp^{\pm}$ mice were stimulated with anti-CD3/CD28 antibodies for varying amounts of time. Mitochondrial morphologies of $C1qbp^{+/+}$ and $C1qbp^{\pm}$ T cells were detected by confocal microscopy. Scale bar, 5 μm. **B** Mean Fluorescence Intensity (MFI) of the mitochondrial marker Cytochrome C in $C1qbp^{+/+}$ and $C1qbp^{\pm}$ T cells. **C** MFI of MitoTracker Green in $C1qbp^{+/+}$ and $C1qbp^{\pm}$ T cells after stimulation with anti-CD3/CD28 antibodies for 3 days. **D** Protein levels of OPA1, MFN2, Drp1, and C1QBP relative to β-actin, as well as the phosphorylation of Drp1 at Ser616, as analyzed by immunoblotting. Bar graphs show the mean ± S.D. of three independent experiments ($n=3$); $^{*}P<0.05$, $^{**}P<0.01$, $^{***}P<0.001$

Further analysis demonstrated that mice with one allele of *C1qbp* disrupted contained more dysfunctional and exhausted T cells relative to their wild-type littermates. Our results showed that $C1qbp^{\pm}$ TILs exhibited higher expression of inhibitory receptors like PD-1, Tim-3, and LAG-3 than the corresponding $C1qbp^{+/+}$ TILs (Fig. 2D). We also assessed the expression of PD-1 and Tim-3 in $CD8^{+}$ T cells from the spleen of $C1qbp^{+/+}$ and $C1qbp^{\pm}$ mice, but observed similarly low expression of such exhaustion molecules in the peripheral T cells between these mice (S. Fig. 4). This distinction suggests that the impact of C1QBP on T cell exhaustion is mainly restricted to the TME, where TILs are exposed to a great deal of metabolic stress. Our results revealed that the intact expression of *C1qbp* is important for prevention of TILs exhaustion and hypofunction.

Together, knocking down *C1qbp* dampened T cell antitumor immune responses by decreasing the proportion of $CD44^{hi}CD62L^{hi}$ central memory T cells, diminishing the tumor-infiltrating T cells, and exacerbating their exhausted phenotype.

Knocking down *C1qbp* impairs T cell mitochondrial metabolism

As C1QBP has been reported to regulate cellular bioenergetics and mitochondrial function [23, 30, 31], we hypothesized that C1QBP may also play an important role in T cell mitochondrial metabolism. By measuring OCR and ECAR after stimulation with anti-CD3/CD28 antibodies for two days, we found that $C1qbp^{\pm}$ T cells possessed the lower basal respiration and the maximal respiration but the higher glycolytic capacity and glycotic reserve than the corresponding $C1qbp^{+/+}$ T cells, indicating that knocking down *C1qbp* suppressed mitochondria-mediated OXPHOS rather than glycolysis occurring in the cytoplasm (Fig. 3). In addition, C1QBP deficiency resulted in T cells with more proton leak and less ATP production, implying that C1QBP may be involved with the maintenance of the integrity of the mitochondrial membrane, thus preferring the catabolic pathways rather than the anabolic pathways.

Spare respiratory capacity (SRC) is an important marker used to assess the extra mitochondrial capacity available to produce energy, especially under the conditions of metabolic stress and nutrient depletion [32–34]. Enhancement of SRC endows T cells with long-term survival and persistent immune function, and is particularly applicable in the metabolically stressed, nutrient-deprived TME. Here, we found that $C1qbp^{\pm}$ T cells exhibited lower SRC levels compared to the corresponding $C1qbp^{+/+}$ T cells, suggesting that down-regulation of C1QBP expression attenuated the extra mitochondrial capacity of these T cells. Therefore, knocking down *C1qbp* repressed T cell mitochondrial OXPHOS and ATP production, aggravated mitochondrial proton leak, and diminished SRC levels, which would collectively be expected to impair T cells adaptation to the TME.

Knocking down *C1qbp* impacts T cell mitochondrial morphology

Previous studies have shown that T cell metabolic programming can be attributed to mitochondrial remodeling [2, 35, 36]. Here, we wanted to investigate whether reduced C1QBP expression would induce the alteration of T cell mitochondrial morphology. First, we examined the mitochondrial morphology of $C1qbp^{\pm}$ or $C1qbp^{+/+}$ T cells in response to T cell receptor (TCR) stimulation with anti-CD3/CD28 antibodies, as before. Our results demonstrated that activated $C1qbp^{+/+}$ T cells possessed predominantly elongated and fused mitochondria, especially after 3 days, while $C1qbp^{\pm}$ T cells possessed more fragmented and punctate mitochondria, which was consistent with the lower fluorescence intensity of mitochondrial marker Cytochrome C (Fig. 4A, B). At the same time, $C1qbp^{\pm}$ T cells also had less mitochondrial mass compared with $C1qbp^{+/+}$ T cells, as shown in Fig. 4C.

The highly dynamic fusion and fission processes determining mitochondrial morphology are controlled by a series of regulatory proteins including dynamin-related protein 1 (Drp-1), optic atrophy-1 (OPA1), and mitofusion1/2(Mfn1/2) [37–40]. Specifically, fission is regulated by the GTPase Drp1, which is translocated from cytoplasm to the outer mitochondrial membrane (OMM) upon phosphorylation to split mitochondria [37, 38]. Conversely, fusion is controlled by three-dynamin family GTPases including Mfn1/2 on the OMM and OPA1 on the inner mitochondrial membrane (IMM) [40–42]. To explore the potential mechanisms by which C1QBP regulates T cells mitochondrial morphology, we detected the protein levels of mitochondrial fission protein and fusion proteins, in both $C1qbp^{\pm}$ and $C1qbp^{+/+}$ T cells. As shown in Fig. 4D, we found that C1QBP obviously enhanced not only the expression of the mitochondrial fission protein, Drp1,

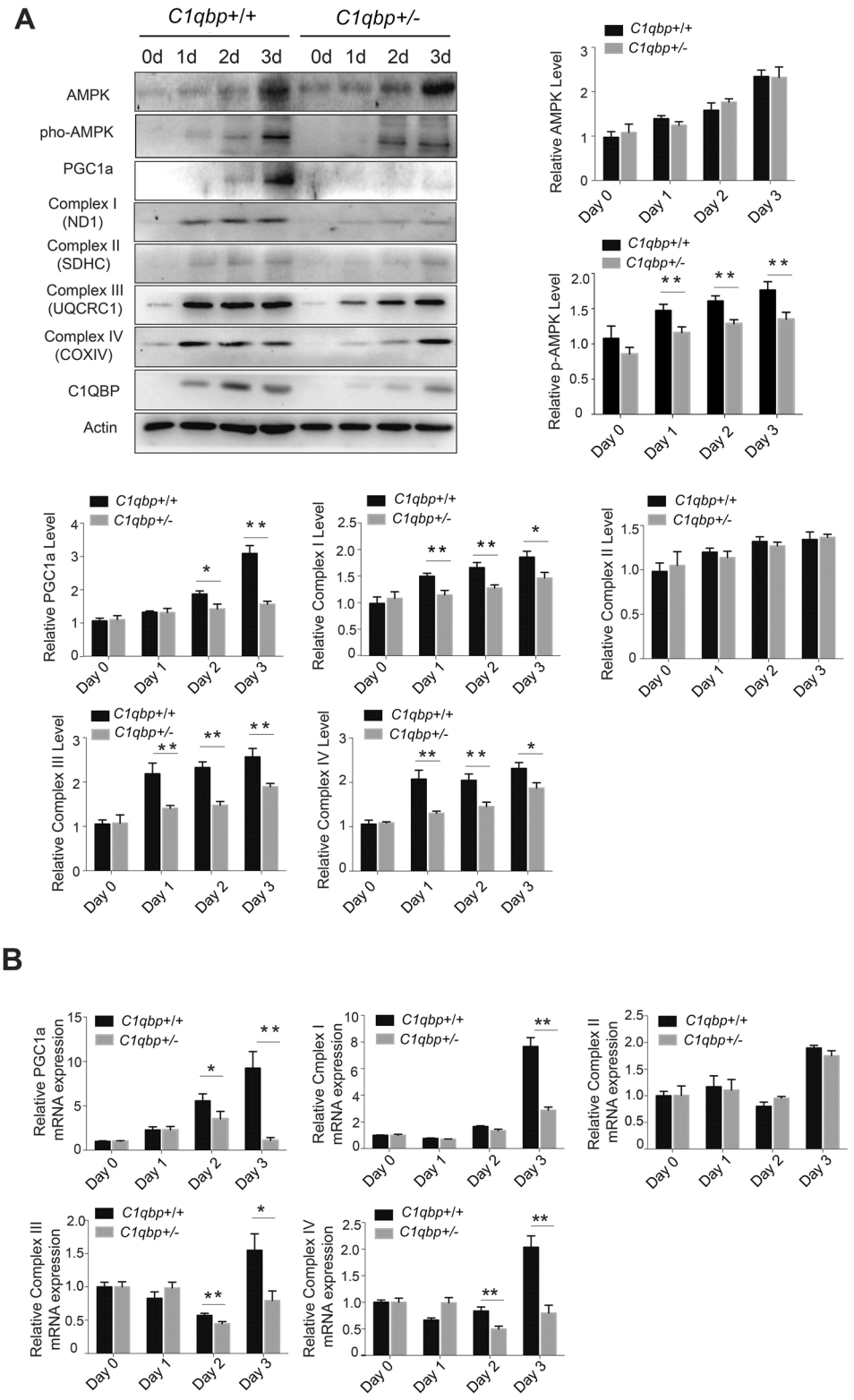

Fig. 5 *C1qbp* knockdown suppresses T cell mitochondrial biogenesis through the AMPK/PGC1α signaling pathway. $C1qbp^{\pm}$ and $C1qbp^{+/+}$ T cells were activated with anti-CD3/CD28 antibodies for the indicated time points. **A** Protein levels of AMPK, PGC1α, Complex I (ND1), Complex II (SDHC), Complex III (UQCRC1), and Complex IV (COXIV) relative to β-actin, as well as phosphorylation of AMPK at Thr172 were detected by immunoblotting. **B** mRNA levels of PGC1α, Complex I, II, III, and IV relative to β-actin were analyzed using qRT-PCR. Bar graphs show the mean ± S.D. of three independent experiments ($n = 3$); $^{*}P < 0.05$, $^{**}P < 0.01$

but also its phosphorylation on Ser616 which is responsible for the scission of mitochondrial membrane. At the same time, C1QBP insufficiency also resulted in decreased expression of mitochondrial fusion proteins, OPA1 and Mfn2. Together, these data suggest that *C1qbp* knockdown resulted in a preference for mitochondrial fission through the increase of Drp1 expression and its phosphorylation on

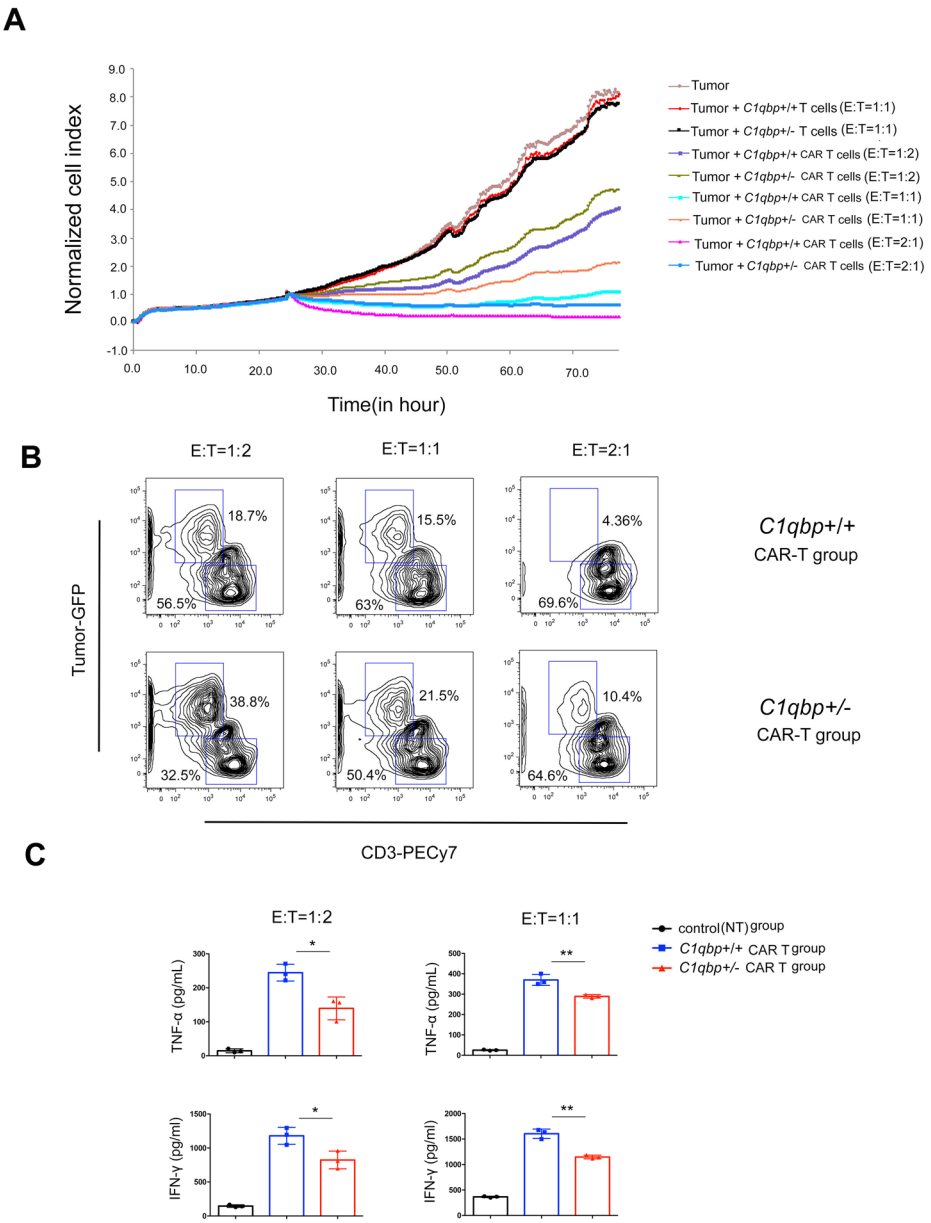

Fig. 6 *C1qbp* knockdown decreases the antitumor immune function of CAR T cells in vitro. **A** HuB7-H3-B16 cells (1×10^4) were seeded on a 16-well micro-E-plate for 24 h, and then co-cultured with non-transduced T cells (*E*:*T* = 1:1), $C1qbp^{+/+}$, or $C1qbp^{\pm}$ CAR T cells targeting the huB7-H3 antigen (*E*:*T* = 1:2, 1:1, and 2:1) for an additional 72 h. Survival of huB7-H3-B16 cells was monitored using the real time RTCA assay. **B** HuB7-H3-B16 cells (2×10^5) were seeded on a 24-well plate for 24 h, and then co-cultured with $C1qbp^{+/+}$ or $C1qbp^{\pm}$ CAR T cells for an additional 6 h (*E*:*T* = 1:2, 1:1, and 2:1). The percentages of residual huB7-H3-B16 tumor cells (GFP^+) and CAR T cells ($PE\text{-}Cy7\text{-}CD3^+$) were estimated by flow cytometry. **C** $C1qbp^{+/+}$ and $C1qbp^{\pm}$ CAR T cells targeting huB7-H3 were co-cultured with huB7-H3 B16 tumor cells (2×10^5 cells/well) in 24-well plates at different effector to target ratios (*E*:*T* = 1:2 or 1:1) without the addition of exogenous cytokines. After 18 h, the supernatant was collected and IFN-γ and TNF-α cytokines were measured in duplicate using specific ELISA kits. Bar graphs show the mean ± S.D. of three independent experiments ($n = 3$); $^*P < 0.05$, $^{**}P < 0.01$

Ser616 as well as the decrease of OPA1 and Mfn2 protein levels.

C1QBP is required to maintain T cell mitochondrial biogenesis through the AMPK/PGC1α signaling pathway

Given that the regulation of mitochondrial dynamics is connected with the alteration of mitochondrial biogenesis [24], we further interrogated whether *C1qbp* knockdown would impact T cell mitochondrial proliferation. Peroxisome proliferator-activated receptor γ coactivator 1α (PGC-1α) has been proposed to play a central role in regulation of mitochondrial biogenesis [43]. Here, our results showed that *C1qbp* knockdown dramatically diminished the transcription and translation of PGC1α, as shown in Fig. 5A–B. On the other hand, AMP-activated protein kinase (AMPK), as a conserved Ser/Thr kinase, is activated by the cellular AMP/ATP ratio and is accordingly involved with the bioenergetic switches from anabolic to catabolic pathways [44]. Moreover, AMPK activation enhances PGC1α expression to promote mitochondrial protein synthesis [45–47]. In this study, we also detected and compared the protein levels and phosphorylation status of AMPK between $C1qbp^{\pm}$ and $C1qbp^{+/+}$ T cells (Fig. 5A). Our data showed that AMPK protein levels gradually increased accompanying with the stimulation of anti-CD3/CD28 antibodies in both $C1qbp^{\pm}$ and $C1qbp^{+/+}$ T cells, with no detectable differences between these populations. However, $C1qbp^{\pm}$ T cells were observed

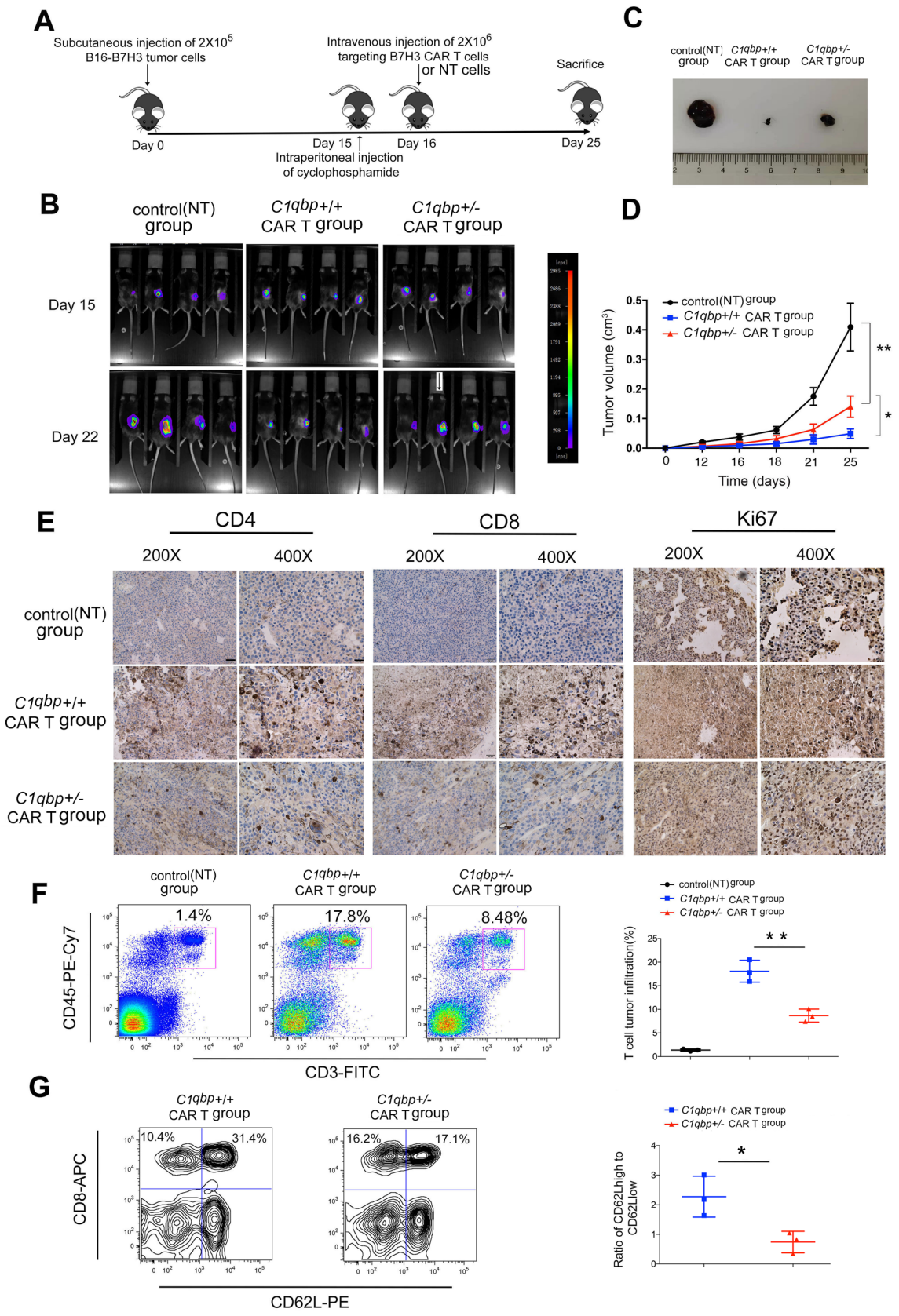
A
Subcutaneous injection of 2X10^5 B16-B7H3 tumor cells
Intravenous injection of 2X10^6 targeting B7H3 CAR T cells or NT cells
Sacrifice
Day 0
Day 15
Day 16
Day 25
Intraperitoneal injection of cyclophosphamide
C
control(NT) group
C1qbp+/+ CAR T group
C1qbp+/- CAR T group
B
control(NT) group
C1qbp+/+ CAR T group
C1qbp+/- CAR T group
Day 15
Day 22
D
control(NT) group
C1qbp+/+ CAR T group
C1qbp+/- CAR T group
Tumor volume (cm3)
Time (days)
**
*
E
CD4
CD8
Ki67
200X
400X
control(NT) group
C1qbp+/+ CAR T group
C1qbp+/- CAR T group
F
control(NT) group
C1qbp+/+ CAR T group
C1qbp+/- CAR T group
1.4%
17.8%
8.48%
CD45-PE-Cy7
CD3-FITC
T cell tumor infiltration(%)
**
G
C1qbp+/+ CAR T group
C1qbp+/- CAR T group
10.4%
31.4%
16.2%
17.1%
CD8-APC
CD62L-PE
Ratio of CD62Lhigh to CD62Llow
*

◂**Fig. 7** *C1qbp* knockdown attenuates CAR T cell immunotherapeutic efficacy in a huB7-H3-B16 subcutaneous xenograft mouse model. **A** Schematic representation of the procedure. Mice received subcutaneous inoculation of huB7-H3-B16 tumor (Day 0), and adoptive transfer of non-transduced control T cells (NT), $C1qbp^{+/+}$, or $C1qbp^{\pm}$ CAR T cells (Day 16) (4 mice/group). **B** Representative bioluminescence images of the mice in each group before (Day 15) and after (Day 22) inoculation of NT, $C1qbp^{+/+}$, or $C1qbp^{\pm}$ CAR T cells. **C** Representative images of the huB7-H3-B16 tumors on Day 25. **D** Volumes of huB7-H3-B16 tumors across groups. **E** Representative CD4, CD8, and Ki67 immunohistochemistry staining of tumors across groups. Scale bars, 50 μm (200×), 20 μm (400×). **F** Relative percentages of TILs across groups, as assessed by flow cytometry. **G** Proportions of $CD62L^{hi}$ and $CD62L^{lo}$ $CD8^+$ T cells in mice who received $C1qbp^{+/+}$ and $C1qbp^{\pm}$ CAR T cells, as assessed by flow cytometry. Bar graphs show the mean ± S.D. of three independent experiments ($n=3$); $^*P<0.05$, $^{**}P<0.01$

to exhibit lower phosphorylation of AMPK on Thr172 when compared to $C1qbp^{+/+}$ T cells. Therefore, it is likely that *C1qbp* knockdown at least partly contributed to a decrease of PGC1α via reduced phosphorylation of AMPK.

Whether the PGC1α signaling pathway regulates T cell mitochondrial protein synthesis still remains unclear. As such, we detected the transcription and translation of mitochondrial proteins, such as the electron transport chain (ETC) complexes I, II, III, and IV, between $C1qbp^{\pm}$ and $C1qbp^{+/+}$ T cells in response to the anti-CD3/CD28-induced TCR stimulation. Our data showed that *C1qbp* knockdown impaired the transcription and translation of the mitochondrial ETC complexes I, III, and IV, which is consistent with the results of the previous studies [11, 48]. Consequently, these data suggest that C1QBP pivotally supports translation of the mitochondrially encoded respiratory chain protein complexes. In order to further explore whether C1QBP could regulate mitochondrial protein synthesis through the PGC1α signaling pathway, we treated $C1qbp^{+/+}$ T cells with PGC1α siRNA and observed the expression of mitochondrial ETC complexes I, III, and IV. Our results showed that PGC1α siRNA repressed the expression level of these mitochondrial proteins even in the context of intact *C1qbp*, as shown in S. Fig. 5. In other words, PGC1α played a pivotal role in C1QBP-mediated mitochondrial biogenesis in response to TCR stimulation. Taken together, C1QBP insufficiency impaired T cell mitochondrial biogenesis and mitochondrial protein synthesis through the AMPK/PGC1α signaling pathway.

Knocking down *C1qbp* attenuates CAR T cells immunotherapeutic efficacy

In order to explore whether C1QBP would directly impact T cell antitumor functions, we constructed CAR T cells with one or two functional copies of *C1qbp*. B7-H3, as a member of the B7 family of immune co-stimulatory and co-inhibitory proteins, possesses two isoforms in humans: 2Ig-B7-H3 and 4Ig-B7-H3. B7-H3 protein exhibits limited expression in normal human tissues, such as those of the liver, breast, and colon, for example, but it exhibits abnormally high expression in the corresponding malignant tissues of these areas [49–51]. Moreover, CAR T cells targeting huB7-H3 were recently reported to exhibit potent antitumor effects on hematologic and solid tumors [52–54]. Here, we assessed $C1qbp^{\pm}$ and $C1qbp^{+/+}$ CAR T cells targeting huB7-H3 to delineate the effect of C1QBP on CAR T cell antitumor efficacy. First, we monitored CAR T-mediated killing of melanoma huB7-H3-B16 cells via the real-time cell analysis (RTCA) and found that $C1qbp^{\pm}$ CAR T cells exhibited weaker cytotoxicity than $C1qbp^{+/+}$ CAR T cells at different effector to target ratios (*E*:*T*), such as 1:2, 1:1 and 2:1, as shown in Fig. 6A. HuB7-H3-B16 cells co-cultured with huB7-H3-targeting CAR T cells also exhibited a similar trend. $C1qbp^{+/+}$ CAR T cells repressed tumor cells to 18.7% (*E*:*T* = 1:2), 15.5% (*E*:*T* = 1:1) and 4.36% (*E*:*T* = 2:1), while $C1qbp^{\pm}$ CAR T cells only controlled tumor cells to 38.8%, 21.5% and 10.4% under the same conditions (Fig. 6B). Additionally, $C1qbp^{\pm}$ CAR T cells released less TNF-α and IFN-γ than $C1qbp^{+/+}$ CAR T cells at different E:*T* ratios (1:2 or 1:1) (Fig. 6C). Together, these results suggest *C1qbp* knockdown attenuated CAR T cells antitumor immune functions in vitro.

To confirm the effect of C1QBP in CAR T cells immunotherapy in vivo, we inoculated huB7-H3-B16 cells into the flanks of C57BL/6 mice and then adoptively transferred $C1qbp^{+/+}$ and $C1qbp^{\pm}$ CAR T cells to assess the impact of this change on tumor progression of these recipient mice. First, mice receiving either of these CAR T cells treatment exhibited significant tumor suppression compared with mice receiving the control non-transduced T cells (NT), suggesting that both CAR T cells targeting huB7-H3 could exert some antitumor immune function. Importantly, though, mice receiving $C1qbp^{\pm}$ CAR T cells exhibited relatively weaker tumor regression than those receiving $C1qbp^{+/+}$ CAR T cells in both the subcutaneous xenograft model as well as the metastasis model of B16 murine melanoma, as shown in Figs. 7B–D and 8B–C. Moreover, our results confirmed that the more Ki67 expressed on tumor cells and the fewer tumor-infiltrating T cells were detected in TME from $C1qbp^{\pm}$ CAR T group, as shown in Figs. 7E–F and 8D–E. At the same time, $C1qbp^{\pm}$ CAR TILs possessed relatively lower mitochondrial mass compared with the corresponding $C1qbp^{+/+}$ CAR TILs (S. Fig. 6). We also assessed the relative ratios of two distinct subsets of memory T cells: central memory T cells ($CD62L^{hi}$) and effector memory T cells ($CD62L^{lo}$). Notably, mice receiving $C1qbp^{\pm}$ CAR T cells exhibited a significantly lower ratio of $CD62L^{hi}$ to $CD62L^{lo}$ than those receiving $C1qbp^{+/+}$ CAR T cells, suggesting that *C1qbp* knockdown inhibited CAR T cells from forming into the central memory phenotype (Figs. 7G, 8F). Further,

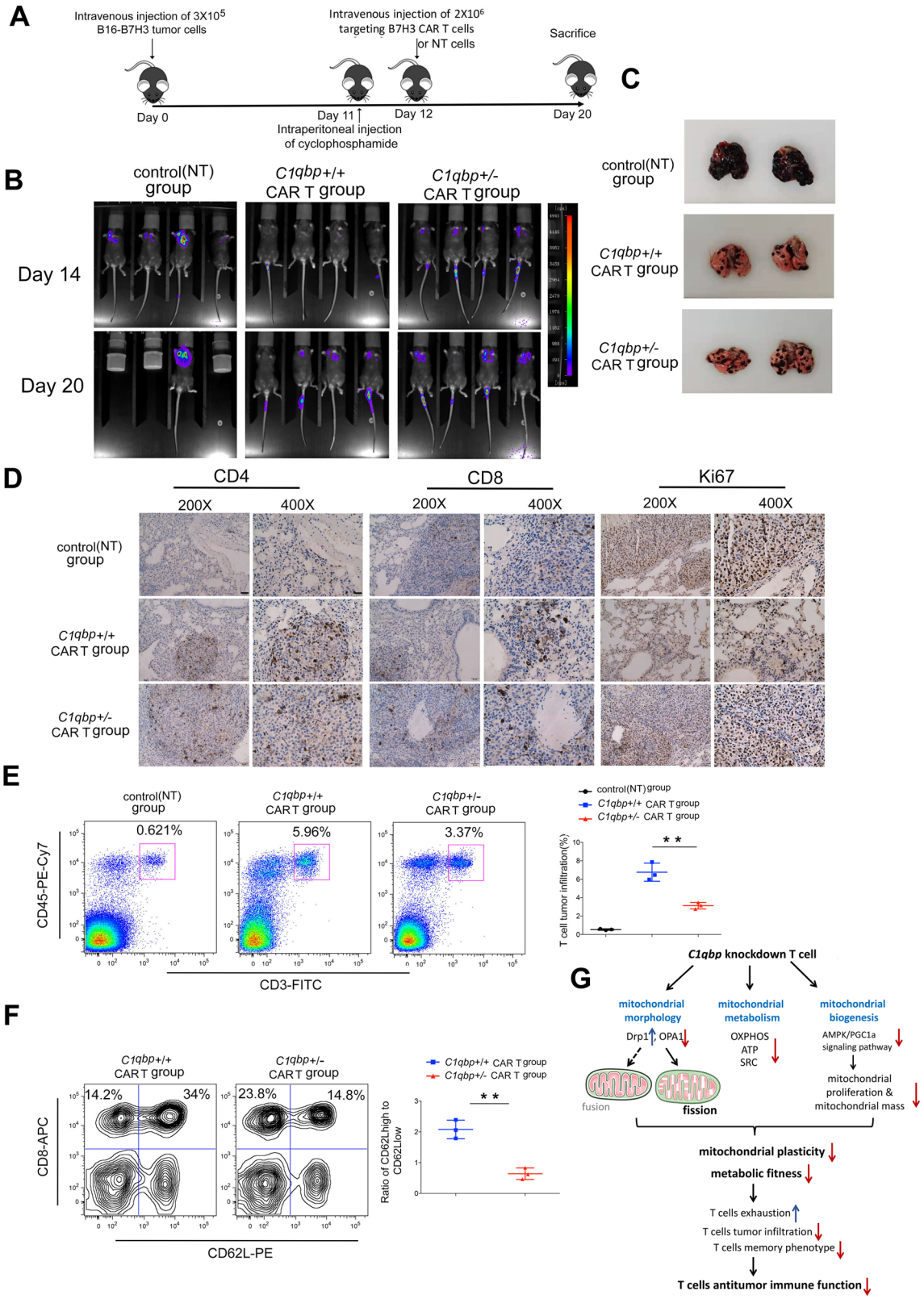

C1qbp$^{\pm}$ CAR TILs exhibited relatively higher expression of the inhibitory receptor, PD-1, in the tumor but not in the spleen (S. Fig. 7A, B), suggesting that *C1qbp* knockdown aggravated the exhausted phenotype of the tumor-infiltrating CAR T cells but not that of the peripheral CAR T cells. Taken together, down-regulation of C1QBP attenuated CAR

◂**Fig. 8** *C1qbp* knockdown dampens CAR T cell immunotherapeutic efficacy in a huB7-H3-B16 metastasis mouse model. **A** Schematic representation of the procedure. Mice received intravenous inoculation of huB7-H3-B16 tumor cells (Day 0), and adoptive transfer of non-transduced control T cells (NT), *C1qbp*$^{+/+}$, or *C1qbp*$^{\pm}$ CAR T cells (Day 12) (4 mice/group). **B** Representative bioluminescent images of the mice in each group on Days 14 & 20. **C** Representative images of the lung tissue across groups. **D** Representative CD4, CD8, and Ki67 immunohistochemistry staining of the lung tissues across groups. Scale bars, 50 μm (200×), 20 μm (400×). **E** Relative percentages of TILs across groups, as assessed by flow cytometry. **F** Proportions of CD62L^{hi} and CD62L^{lo} CD8^{+} T cells in mice who received *C1qbp*$^{+/+}$ or *C1qbp*$^{\pm}$ CAR T cells, as assessed by flow cytometry. **G** Schematic model of the impact of *C1qbp* knockdown on T cell antitumor immune function. Bar graphs show the mean ± S.D. of three independent experiments ($n = 3$); $^{*}P < 0.05$, $^{**}P < 0.01$

T cell tumor infiltration and central memory cell formation and exacerbated their exhausted phenotype in the TME, thus dampening their corresponding immunotherapeutic efficacy in vivo.

Discussion

Mitochondria as dynamic organelles are critical for the tuning of metabolic preferences in response to environmental stimuli, which are, in turn, critical in orchestrating T cell development, fate, and function. Indeed, Zhai et al. presented important evidence of a critical role for *C1qbp* in the differentiation of effector CD8^{+} T cells through a metabolic-epigenetic axis, suggesting that *C1qbp* deficiency-mediated mitochondrial dysfunction can induce metabolic and epigenetic reprograming of T cell differentiation [55]. However, recent studies have also pointed out that dysfunctional mitochondria with decreased metabolic fitness can drive permanent T cell dysfunction in the TME [3, 4, 24]. Consequently, we sought to explore the relationship between C1QBP-mediated mitochondrial rewiring and T cell antitumor immune function. Here, mitochondrial plasticity was used to evaluate mitochondrial adaptation and metabolic fitness in response to a challenging microenvironment. Given that multiple tumor microenvironmental factors are involved in the development of TIL exhaustion, mitochondrial plasticity helps T cells to cope with a variety of metabolic stressors, including glucose competition, metabolite accumulation, chronic tumor antigenic stimulation through the TCR, hypoxia, and checkpoint signaling such as the PD-1/PD-L1 pathway. In this study, we demonstrated that *C1qbp* knockdown impaired mitochondrial plasticity by increasing mitochondrial fission, decreasing mitochondrial metabolism, and diminishing mitochondrial biogenesis, all of which subsequently impacted T cell exhaustion and central memory cell generation to ultimately dampen their persistent antitumor immune function.

Mitochondrial dynamics, including remodeling of mitochondrial architecture, mass, and activity, are important drivers for appropriate metabolic reprogramming in response to metabolic perturbations. Mitochondrial fusion allows T cells to support metabolic demands, while mitochondrial fission impairs T cells mitochondrial functions and represses their antitumor immunity [2]. Our data showed that the mitochondrial protein C1QBP is a critical regulator in the modulation of T cell mitochondrial morphology. *C1qbp*$^{\pm}$ T cells possessed more punctate and fragmented mitochondria, while *C1qbp*$^{+/+}$ T cells had more tubular and fused mitochondria in response to stimulation with anti-CD3/CD28 antibodies. Moreover, we found that *C1qbp* knockdown increased levels of the mitochondrial fission protein Drp1 as well as its phosphorylation on Ser616, and also repressed the mitochondrial fusion proteins OPA1 and Mfn2. These data suggest that reduced C1QBO expression rendered T cells prone to mitochondrial fission, which attenuates the ability of T cells to adapt to the relentlessly challenging TME.

In fact, emerging evidence has delineated the importance of this intricate balance between mitochondrial fission and fusion on T cell metabolism and immune function [56–58]. Pearce et al. [2] found that fused mitochondria had tight cristae, which yielded more efficient ETC activity and favored OXPHOS as well as FAO, while fragmented mitochondria had the loose cristae, which exhibited less efficient ETC activity and thus favored aerobic glycolysis. Inhibition of mitochondrial OXPHOS has also been shown to result in the suppression of CD8^{+} T cell memory formation as well as upregulation their exhaustion [4]. In our study, *C1qbp*$^{\pm}$ T cells exhibited more fragmented mitochondria and lower OXPHOS as well as less ATP production, which decreased TIL metabolic fitness. Notably, enhanced mitochondrial SRC was also thought to be an important property for cells to achieve long-term survival and efficacy [34, 59]. In this study, *C1qbp*$^{\pm}$ T cells exhibited weakened SRC relative to *C1qbp*$^{+/+}$ T cells, which suggested down-regulation of C1QBP rendered T cells with less extra mitochondrial capacity to meet bioenergetic demands. On the other hand, C1QBP insufficiency repressed the relative ratio of CD44^{hi}CD62L^{hi} central memory to CD44^{hi}CD62L^{lo} effector memory T cells. Similarly, tumor-bearing mice receiving tumor-specific *C1qbp*$^{\pm}$ CAR T cells exhibited lower proportions of the central memory phenotype when compared to their *C1qbp*$^{+/+}$ CAR T cells, although this effect, importantly, was only true for TILs but not for peripheral T cells. Consequently, how and whether C1QBP enhancement could promote mitochondrial metabolism and SRC to drive central memory T cell formation remains to be elucidated.

Indeed, the previous study reported that C1QBP deficient mice exhibited mid-gestation lethality due to the severe dysfunction of the mitochondrial respiratory chain

[23]. They further found that C1QBP bound RNA and interacted with mitochondrial messenger RNA species in vivo. Moreover, co-immunoprecipitation revealed the close association of C1QBP with the mitoribosome. This RNA-binding ability of C1QBP was well correlated with mitochondrial translation. However, in our study, we found that *C1qbp* knockdown repressed the synthesis of the mitochondrial ETC proteins, complexes I, III, and IV. Reduced C1QBP expression also resulted in the decrease of T cell mitochondrial mass in vitro and in vivo. In this regard, C1QBP not only takes a crucial role in mtDNA translation through the association with mitoribosome, but also regulates the AMPK/PGC1a signaling axis to modulate mitochondrial proliferation.

Given that tumor specific T cells frequently exhibit decreased mitochondrial biogenesis, metabolic reprogramming via enhancement of PGC1α expression was reported to be correlated with reinvigoration of mitochondrial function and improvement of T cell antitumor responses [24, 60]. In this study, *C1qbp* knockdown exacerbated the expression of inhibitory receptors, PD-1, Tim-3, and LAG-3, in TILs. Given that TILs with a progressive loss of PGC1α have been shown to lack mitochondrial biogenesis, and that enhancement of PGC1α has been shown to contribute to metabolic plasticity and effector function [24], we presumed that C1QBP-mediated PGC1α upregulation could trigger metabolic reprogramming in TILs, which could reinvigorate their mitochondrial plasticity to resist exhaustion and hypofunction in the TME. Intriguingly, Bengsch et al. reported that PD-1 repressed PGC1α, while improving bioenergetics by overexpression of PGC1α prevented T cell exhaustion, in turn inducing the anti-PD-L1 therapeutic reinvigoration by reprogramming metabolism in the subset of PD-1^{Int} exhausted T cells [60]. T cells with features of more severe exhaustion exhibit a specialized DNA methylation pattern and chromatin architecture that may lock T cells in a permanently dysfunctional state, and are refractory to anti-PD-1 treatment. However, the transcription factor T cell factor 1 (TCF1) endows T cells with a stem-like phenotype by triggering the distinct transcriptomic and epigenetic regulation, which further contributes to a proliferative burst upon PD-1 blockade treatment [61–63]. Therefore, the development of novel, effective strategies to reprogram mitochondrial functions will improve the current response to such checkpoint blockade therapies. In this regard, how and whether C1QBP-mediated PGC1α enhancement could trigger TCF1 expression, and thus induce additive antitumor immunity when used in conjunction with anti-PD-1 checkpoint blockade, warrants further evaluation.

Taken together, as shown in Fig. 8G, C1qbp knockdown resulted in T cells with more mitochondrial fission, lower mitochondrial OXPHOS, and weaker mitochondrial biogenesis, together attenuating mitochondrial plasticity and metabolic fitness and thus exerting a negative impact on T cell tumor infiltration, exhaustion, and memory phenotype formation. In this regard, improvement of mitochondrial plasticity through C1QBP might endow T cells or CAR T cells with robust and persistent antitumor functions, which may present a novel strategy to promote their antitumor immunotherapeutic efficacy.

Supplementary Information The online version contains supplementary material available at https://doi.org/10.1007/s00262-023-03407-5.

Acknowledgements This work was supported by the National Natural Science Foundation of China (Nos. 82073012, 81871869, 81872488, 81803080, 32200124), the National Key R&D Program of China (No. 2018YFA0900900), the Key University Science Research Project of Jiangsu Province (No. 19KJA580001), the Natural Science Foundation of the Jiangsu Higher Education Institutions of China (18KJA320013), the Natural Science Foundation of Jiangsu Province (BK20180990), the Jiangsu Young Medical Talents Project, the Jiangsu Provincial Key Medical Discipline, and the Project of Invigorating Health Care through Science, Technology, and Education (No. ZDXKA2016014).

Author contributions Conception and design: HT, ZG, and JNZ; development of methodology: HT, DC, GW, QW, and JS; acquisition of data and critical reagents, animals and facility support: HL, NS, GJ, JS, and LF; analysis and interpretation of data (statistical analysis, biostatistics computational analysis): HT, DC, GW, NS, and QW; writing, review, and/or revision of the manuscript: HT, DC, GW, QW, and ZG; administrative, technical or material support (reporting or organizing data, constructing databases): HL, NS, LF, and MW; study supervision: ZG.

Declarations

Conflict of interest The authors declare no conflict of interests.

References

1. Liu X, Peng G (2021) Mitochondria orchestrate T cell fate and function. Nat Immunol 22:276–278. https://doi.org/10.1038/s41590-020-00861-6
2. Buck MD, O'Sullivan D, Klein Geltink RI et al (2016) Mitochondrial dynamics controls T cell fate through metabolic programming. Cell 166:63–76. https://doi.org/10.1016/j.cell.2016.05.035
3. Yu YR, Imrichova H, Wang H et al (2020) Disturbed mitochondrial dynamics in CD8(+) TILs reinforce T cell exhaustion. Nat Immunol 21:1540–1551. https://doi.org/10.1038/s41590-020-0793-3
4. Vardhana SA, Hwee MA, Berisa M et al (2020) Impaired mitochondrial oxidative phosphorylation limits the self-renewal of T cells exposed to persistent antigen. Nat Immunol 21:1022–1033. https://doi.org/10.1038/s41590-020-0725-2
5. Ma K, Chen G, Li W, Kepp O, Zhu Y, Chen Q (2020) Mitophagy, mitochondrial homeostasis, and cell fate. Front Cell Dev Biol 8:467. https://doi.org/10.3389/fcell.2020.00467
6. Bahat A, Gross A (2019) Mitochondrial plasticity in cell fate regulation. J Biol Chem 294:13852–13863. https://doi.org/10.1074/jbc.REV118.000828

7. Popov LD (2020) Mitochondrial biogenesis: an update. J Cell Mol Med 24:4892–4899. https://doi.org/10.1111/jcmm.15194
8. Tian H, Zhang B, Li L, Wang G, Li H, Zheng J (2020) Manipulation of mitochondrial plasticity changes the metabolic competition between "foe" and "friend" during tumor malignant transformation. Front Oncol 10:1692. https://doi.org/10.3389/fonc.2020.01692
9. Lanna A, Dustin ML (2016) Mitochondrial fusion fuels T cell memory. Cell Res 26:969–970. https://doi.org/10.1038/cr.2016.94
10. Li Y, Wan OW, Xie W, Chung KK (2011) p32 regulates mitochondrial morphology and dynamics through parkin. Neuroscience 199:346–358. https://doi.org/10.1016/j.neuroscience.2011.10.003
11. Fogal V, Richardson AD, Karmali PP, Scheffler IE, Smith JW, Ruoslahti E (2010) Mitochondrial p32 protein is a critical regulator of tumor metabolism via maintenance of oxidative phosphorylation. Mol Cell Biol 30:1303–1318. https://doi.org/10.1128/MCB.01101-09
12. Amamoto R, Yagi M, Song Y et al (2011) Mitochondrial p32/C1QBP is highly expressed in prostate cancer and is associated with shorter prostate-specific antigen relapse time after radical prostatectomy. Cancer Sci 102:639–647. https://doi.org/10.1111/j.1349-7006.2010.01828.x
13. Kohda M, Tokuzawa Y, Kishita Y et al (2016) A comprehensive genomic analysis reveals the genetic landscape of mitochondrial respiratory chain complex deficiencies. PLoS Genet 12:e1005679. https://doi.org/10.1371/journal.pgen.1005679
14. Zhang X, Zhang F, Guo L, Wang Y, Zhang P, Wang R, Zhang N, Chen R (2013) Interactome analysis reveals that C1QBP (complement component 1, q subcomponent binding protein) is associated with cancer cell chemotaxis and metastasis. Mol Cell Proteom 12:3199–3209. https://doi.org/10.1074/mcp.M113.029413
15. Breda CNS, Davanzo GG, Basso PJ, Saraiva Camara NO, Moraes-Vieira PMM (2019) Mitochondria as central hub of the immune system. Redox Biol 26:101255. https://doi.org/10.1016/j.redox.2019.101255
16. Pearce EJ, Pearce EL (2018) Immunometabolism in 2017: driving immunity: all roads lead to metabolism. Nat Rev Immunol 18:81–82. https://doi.org/10.1038/nri.2017.139
17. Geltink RIK, Kyle RL, Pearce EL (2018) Unraveling the complex interplay between T cell metabolism and function. Annu Rev Immunol 36:461–488. https://doi.org/10.1146/annurev-immunol-042617-053019
18. Youle RJ, van der Bliek AM (2012) Mitochondrial fission, fusion, and stress. Science 337:1062–1065. https://doi.org/10.1126/science.1219855
19. Jheng HF, Tsai PJ, Guo SM, Kuo LH, Chang CS, Su IJ, Chang CR, Tsai YS (2012) Mitochondrial fission contributes to mitochondrial dysfunction and insulin resistance in skeletal muscle. Mol Cell Biol 32:309–319. https://doi.org/10.1128/MCB.05603-11
20. Molina AJ, Wikstrom JD, Stiles L et al (2009) Mitochondrial networking protects beta-cells from nutrient-induced apoptosis. Diabetes 58:2303–2315. https://doi.org/10.2337/db07-1781
21. Rambold AS, Cohen S, Lippincott-Schwartz J (2015) Fatty acid trafficking in starved cells: regulation by lipid droplet lipolysis, autophagy, and mitochondrial fusion dynamics. Dev Cell 32:678–692. https://doi.org/10.1016/j.devcel.2015.01.029
22. Rambold AS, Kostelecky B, Elia N, Lippincott-Schwartz J (2011) Tubular network formation protects mitochondria from autophagosomal degradation during nutrient starvation. Proc Natl Acad Sci U S A 108:10190–10195. https://doi.org/10.1073/pnas.1107402108
23. Yagi M, Uchiumi T, Takazaki S, Okuno B, Nomura M, Yoshida S, Kanki T, Kang D (2012) p32/gC1qR is indispensable for fetal development and mitochondrial translation: importance of its RNA-binding ability. Nucleic Acids Res 40:9717–9737. https://doi.org/10.1093/nar/gks774
24. Scharping NE, Menk AV, Moreci RS, Whetstone RD, Dadey RE, Watkins SC, Ferris RL, Delgoffe GM (2016) The tumor microenvironment represses T cell mitochondrial biogenesis to drive intratumoral T cell metabolic insufficiency and dysfunction. Immunity 45:374–388. https://doi.org/10.1016/j.immuni.2016.07.009
25. Siska PJ, Beckermann KE, Mason FM et al (2017) Mitochondrial dysregulation and glycolytic insufficiency functionally impair CD8 T cells infiltrating human renal cell carcinoma. JCI Insight. https://doi.org/10.1172/jci.insight.93411
26. Gotoh K, Morisaki T, Setoyama D et al (2018) Mitochondrial p32/C1qbp is a critical regulator of dendritic cell metabolism and maturation. Cell Rep 25:180-15e4. https://doi.org/10.1016/j.celrep.2018.10.057
27. Liu Y, Leslie PL, Jin A, Itahana K, Graves LM, Zhang Y (2018) p32 regulates ER stress and lipid homeostasis by down-regulating GCS1 expression. FASEB J 32:3892–3902. https://doi.org/10.1096/fj.201701004RR
28. Tian H, Wang G, Wang Q et al (2022) Complement C1q binding protein regulates T cells' mitochondrial fitness to affect their survival, proliferation, and anti-tumor immune function. Cancer Sci 113:875–890. https://doi.org/10.1111/cas.15261
29. Du H, Hirabayashi K, Ahn S et al (2019) Antitumor responses in the absence of toxicity in solid tumors by targeting B7-H3 via chimeric antigen receptor T cells. Cancer Cell 35:221-37e8. https://doi.org/10.1016/j.ccell.2019.01.002
30. Hu M, Crawford SA, Henstridge DC, Ng IH, Boey EJ, Xu Y, Febbraio MA, Jans DA, Bogoyevitch MA (2013) p32 protein levels are integral to mitochondrial and endoplasmic reticulum morphology, cell metabolism and survival. Biochem J 453:381–391. https://doi.org/10.1042/BJ20121829
31. Muta T, Kang D, Kitajima S, Fujiwara T, Hamasaki N (1997) p32 protein, a splicing factor 2-associated protein, is localized in mitochondrial matrix and is functionally important in maintaining oxidative phosphorylation. J Biol Chem 272:24363–24370. https://doi.org/10.1074/jbc.272.39.24363
32. Choi SW, Gerencser AA, Nicholls DG (2009) Bioenergetic analysis of isolated cerebrocortical nerve terminals on a microgram scale: spare respiratory capacity and stochastic mitochondrial failure. J Neurochem 109:1179–1191. https://doi.org/10.1111/j.1471-4159.2009.06055.x
33. Ferrick DA, Neilson A, Beeson C (2008) Advances in measuring cellular bioenergetics using extracellular flux. Drug Discov Today 13:268–274. https://doi.org/10.1016/j.drudis.2007.12.008
34. van der Windt GJ, Everts B, Chang CH, Curtis JD, Freitas TC, Amiel E, Pearce EJ, Pearce EL (2012) Mitochondrial respiratory capacity is a critical regulator of CD8+ T cell memory development. Immunity 36:68–78. https://doi.org/10.1016/j.immuni.2011.12.007
35. Cogliati S, Frezza C, Soriano ME et al (2013) Mitochondrial cristae shape determines respiratory chain supercomplexes assembly and respiratory efficiency. Cell 155:160–171. https://doi.org/10.1016/j.cell.2013.08.032
36. Mishra P, Carelli V, Manfredi G, Chan DC (2014) Proteolytic cleavage of Opa1 stimulates mitochondrial inner membrane fusion and couples fusion to oxidative phosphorylation. Cell Metab 19:630–641. https://doi.org/10.1016/j.cmet.2014.03.011
37. Lee JE, Westrate LM, Wu H, Page C, Voeltz GK (2016) Multiple dynamin family members collaborate to drive mitochondrial division. Nature 540:139–143. https://doi.org/10.1038/nature20555
38. Koch A, Thiemann M, Grabenbauer M, Yoon Y, McNiven MA, Schrader M (2003) Dynamin-like protein 1 is involved in

peroxisomal fission. J Biol Chem 278:8597–8605. https://doi.org/10.1074/jbc.M211761200
39. Chen H, Chomyn A, Chan DC (2005) Disruption of fusion results in mitochondrial heterogeneity and dysfunction. J Biol Chem 280:26185–26192. https://doi.org/10.1074/jbc.M503062200
40. Chen H, Detmer SA, Ewald AJ, Griffin EE, Fraser SE, Chan DC (2003) Mitofusins Mfn1 and Mfn2 coordinately regulate mitochondrial fusion and are essential for embryonic development. J Cell Biol 160:189–200. https://doi.org/10.1083/jcb.200211046
41. Cipolat S, Martins de Brito O, Dal Zilio B, Scorrano L (2004) OPA1 requires mitofusin 1 to promote mitochondrial fusion. Proc Natl Acad Sci U S A 101:15927–15932. https://doi.org/10.1073/pnas.0407043101
42. MacVicar T, Langer T (2016) OPA1 processing in cell death and disease - the long and short of it. J Cell Sci 129:2297–2306. https://doi.org/10.1242/jcs.159186
43. Fernandez-Marcos PJ, Auwerx J (2011) Regulation of PGC-1alpha, a nodal regulator of mitochondrial biogenesis. Am J Clin Nutr 93:884S-S890. https://doi.org/10.3945/ajcn.110.001917
44. Hardie DG (2011) AMP-activated protein kinase: an energy sensor that regulates all aspects of cell function. Genes Dev 25:1895–1908. https://doi.org/10.1101/gad.17420111
45. Jager S, Handschin C, St-Pierre J, Spiegelman BM (2007) AMP-activated protein kinase (AMPK) action in skeletal muscle via direct phosphorylation of PGC-1alpha. Proc Natl Acad Sci U S A 104:12017–12022. https://doi.org/10.1073/pnas.0705070104
46. Canto C, Auwerx J (2009) PGC-1alpha, SIRT1 and AMPK, an energy sensing network that controls energy expenditure. Curr Opin Lipidol 20:98–105. https://doi.org/10.1097/MOL.0b013e328328d0a4
47. Canto C, Gerhart-Hines Z, Feige JN, Lagouge M, Noriega L, Milne JC, Elliott PJ, Puigserver P, Auwerx J (2009) AMPK regulates energy expenditure by modulating NAD+ metabolism and SIRT1 activity. Nature 458:1056–1060. https://doi.org/10.1038/nature07813
48. Yagi M, Uchiumi T, Sagata N, Setoyama D, Amamoto R, Matsushima Y, Kang D (2017) Neural-specific deletion of mitochondrial p32/C1qbp leads to leukoencephalopathy due to undifferentiated oligodendrocyte and axon degeneration. Sci Rep 7:15131. https://doi.org/10.1038/s41598-017-15414-5
49. Kontos F, Michelakos T, Kurokawa T, Sadagopan A, Schwab JH, Ferrone CR, Ferrone S (2021) B7-H3: an attractive target for antibody-based immunotherapy. Clin Cancer Res 27:1227–1235. https://doi.org/10.1158/1078-0432.CCR-20-2584
50. Seaman S, Zhu Z, Saha S et al (2017) Eradication of tumors through simultaneous ablation of CD276/B7-H3-positive tumor cells and tumor vasculature. Cancer Cell 31:501-15e8. https://doi.org/10.1016/j.ccell.2017.03.005
51. Kraan J, van den Broek P, Verhoef C, Grunhagen DJ, Taal W, Gratama JW, Sleijfer S (2014) Endothelial CD276 (B7-H3) expression is increased in human malignancies and distinguishes between normal and tumour-derived circulating endothelial cells. Br J Cancer 111:149–156. https://doi.org/10.1038/bjc.2014.286
52. Majzner RG, Theruvath JL, Nellan A et al (2019) CAR T cells targeting B7-H3, a pan-cancer antigen, demonstrate potent preclinical activity against pediatric solid tumors and brain tumors. Clin Cancer Res 25:2560–2574. https://doi.org/10.1158/1078-0432.CCR-18-0432
53. Tang X, Zhao S, Zhang Y et al (2019) B7-H3 as a novel CAR-T therapeutic target for glioblastoma. Mol Ther Oncolytics 14:279–287. https://doi.org/10.1016/j.omto.2019.07.002
54. Zhang Z, Jiang C, Liu Z et al (2020) B7-H3-targeted CAR-T cells exhibit potent antitumor effects on hematologic and solid tumors. Mol Ther Oncolytics 17:180–189. https://doi.org/10.1016/j.omto.2020.03.019
55. Zhai X, Liu K, Fang H et al (2021) Mitochondrial C1qbp promotes differentiation of effector CD8(+) T cells via metabolic-epigenetic reprogramming. Sci Adv 7:eabk0490. https://doi.org/10.1126/sciadv.abk0490
56. Rambold AS, Pearce EL (2018) Mitochondrial dynamics at the interface of immune cell metabolism and function. Trends Immunol 39:6–18. https://doi.org/10.1016/j.it.2017.08.006
57. Mishra P, Chan DC (2016) Metabolic regulation of mitochondrial dynamics. J Cell Biol 212:379–387. https://doi.org/10.1083/jcb.201511036
58. Wai T, Langer T (2016) Mitochondrial dynamics and metabolic regulation. Trends Endocrinol Metab 27:105–117. https://doi.org/10.1016/j.tem.2015.12.001
59. Nicholls DG (2009) Spare respiratory capacity, oxidative stress and excitotoxicity. Biochem Soc Trans 37:1385–1388. https://doi.org/10.1042/BST0371385
60. Bengsch B, Johnson AL, Kurachi M et al (2016) Bioenergetic insufficiencies due to metabolic alterations regulated by the inhibitory receptor PD-1 are an early driver of CD8(+) T cell exhaustion. Immunity 45:358–373. https://doi.org/10.1016/j.immuni.2016.07.008
61. Chen Z, Ji Z, Ngiow SF et al (2019) TCF-1-centered transcriptional network drives an effector versus exhausted CD8 T cell-fate decision. Immunity 51:840-55e5. https://doi.org/10.1016/j.immuni.2019.09.013
62. Im SJ, Hashimoto M, Gerner MY et al (2016) Defining CD8+ T cells that provide the proliferative burst after PD-1 therapy. Nature 537:417–421. https://doi.org/10.1038/nature19330
63. Siddiqui I, Schaeuble K, Chennupati V et al (2019) Intratumoral Tcf1(+)PD-1(+)CD8(+) T cells with stem-like properties promote Tumor control in response to vaccination and checkpoint blockade immunotherapy. Immunity 50:195-211e10. https://doi.org/10.1016/j.immuni.2018.12.021